

www.acsami.org Research Article

# Amphiphilic Nitroxide-Bearing Siloxane-Based Block Copolymer Coatings for Enhanced Marine Fouling Release

Amanda Leonardi, Aria C. Zhang, Nilay Düzen, Nick Aldred, John A. Finlay, Jessica L. Clarke, Anthony S. Clare, Rachel A. Segalman, and Christopher K. Ober\*



Cite This: ACS Appl. Mater. Interfaces 2021, 13, 28790–28801



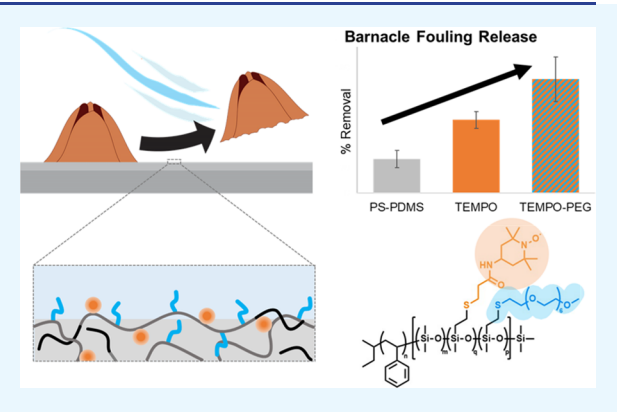
ACCESS

III Metrics & More

Article Recommendations

Supporting Information

ABSTRACT: The buildup of organic matter and organisms on surfaces exposed to marine environments, known as biofouling, is a disruptive and costly process affecting maritime operations. Previous research has identified some of the surface characteristics particularly suited to the creation of antifouling and fouling-release surfaces, but there remains room for improvement against both macrofouling and microfouling organisms. Characterization of their adhesives has shown that many rely on oxidative chemistries. In this work, we explore the incorporation of the stable radical 2,2,6,6-tetramethylpipiderin-1-oxyl (TEMPO) as a component in an amphiphilic block copolymer system to act as an inhibitor for marine cements, disrupting adhesion of macrofouling organisms. Using polystyrene-b-poly(dimethylsiloxane-r-vinylmethysiloxane) block copolymers, pendent vinyl groups were functionalized with TEMPO and poly(ethylene glycol) to construct an amphiphilic material



with redox active character. The antifouling and fouling-release performance of these materials was investigated through settlement and removal assays of three model fouling organisms and correlated to surface structure and chemistry. Surfaces showed significant antifouling character and fouling-release performance was increased substantially toward barnacles by the incorporation of stable radicals, indicating their potential for marine antifouling applications.

KEYWORDS: fouling-release surfaces, antifouling surfaces, block copolymer, polydimethylsiloxane, stable radical, antioxidant, barnacle, algae

#### **■** INTRODUCTION

Marine biofouling is the buildup of organic matter and organisms on surfaces exposed to saltwater environments. On marine vessels, fouling contributes to increased drag,  $^{1,2}$  higher fuel and maintenance costs,  $^3$  and interference in instrument functions  $^4$  and places marine ecosystems at a higher risk of invasive species.  $^5$  The majority of current antifouling technology relies on the use of toxic metal biocides, but increased scrutiny has prompted growing interest in nontoxic, environmentally benign alternatives.  $^{6-10}$ 

To effectively combat marine biofouling without the use of biocides, coatings can operate through two different mechanisms: antifouling or fouling-release behavior. An antifouling coating prevents settlement of organisms on a surface, while a fouling-release coating limits adhesive interaction at the surface to facilitate straightforward removal. Successful antifouling coatings may incorporate hydrophilic materials, such as polyethylene glycol (PEG) or zwitterions, as they create a highly hydrated surface, which makes the adsorption of biomolecules less energetically favorable. 11,12 In contrast, low surface energy materials serve as the best fouling-release coatings because they limit strong polar interactions that

usually adhere foulants to the surface, although diatom slimes are known to stick well to hydrophobic coatings.  $^{13}$  One of the most successful materials for fouling-release coatings is poly(dimethyl siloxane) (PDMS).  $^{14,15}$  The low energy surface limits adhesive interactions, while the soft mechanical properties lower the force necessary to remove settled organisms. Modification of PDMS with hydrophilic materials, like PEG and zwitterions, has shown promise in the construction of surfaces that possess both antifouling and fouling-release capabilities.  $^{16-22}$ 

Many of the cements that marine organisms use for adhesion rely heavily on oxidative mechanisms for cross-linking. Mussels and tubeworms mediate adhesion using catechols, specifically 3,4-dihydroxy phenylalanine (DOPA) residues in their cement, which can form strong bonds with the surface and cross-link

Received: March 21, 2021 Accepted: May 24, 2021 Published: June 9, 2021





within the cement matrix. 23-26 Catechols and oxidases have been identified at the barnacle-adhesive interface as well, but there is mounting evidence that barnacle adhesion is more complex than previously believed, most likely deriving from physiological processes used to produce and maintain tissues. 27-30 Other studies have also shown high concentrations of disulfide linkages in barnacle cement.<sup>31</sup> In a similar vein, certain species of diatoms incorporate high levels of tyrosine in proteins released in their adhesive materials.<sup>32</sup> Directly targeting oxidative mechanisms could serve to improve nontoxic fouling-release performance by interference with physiological adhesive processes. Indeed, Del Grosso et al. investigated the incorporation of antioxidants into an epoxybased paint and found that loadings of 25% antioxidant significantly reduced mussel adhesion strength compared to bare aluminum or a control coating containing 3,5-di-tertbutyltoluene.33

Nitroxides are a class of organic stable radicals that have found applications in organic catalysis and polymer synthesis, 34,35 chemical biology and cell biology, 36,37 and organic electronics.<sup>38</sup> One of the most common nitroxides, 2,2,6,6tetramethylpipiderine-1-oxyl (TEMPO), has been used in antifouling applications to inhibit proliferation and trigger dispersal of biofilms. 39-41 In one study, thin films of poly(2,2,6,6-tetramethylpipiderine-1-oxyl) methacrylate (PTMA) reduced adhesion of Pseudomonas by 99.6% as compared to a poly(methyl methacrylate) control. 42 The mechanism of action is thought to rely on the nitroxide's structural and electronic similarity to nitric oxide, which, in bacteria, is used as a signaling molecule in quorum sensing.<sup>4</sup> Organic nitroxides and their precursors have also long been used as antioxidants and radical scavengers and have been shown to effectively quench hydroxyl, 44-46 peroxyl, 47 carboncentered, 48-50 and thiyl radicals 51 but have yet to be explored for use against macroscopic fouling organisms. Because of this broad-spectrum behavior, nitroxides could be extremely effective additions to a fouling-release coating by quenching any oxidative or radical-based reactions at the adhesive interface, thereby weakening surface attachment.

In this study, a block copolymer system of polystyrene-bpoly(dimethylsiloxane-r-vinylmethysiloxane) (PS-PDMS) was functionalized with TEMPO in order to improve the release of hard foulers. This block copolymer system has been used previously in the construction and study of antifouling and fouling-release coatings, demonstrating the utility of segmental sequence control in marine antifouling 52,53 and elucidating the role of hydrogen bond donors in the fouling release of marine algae. 54,55 Since hydrophobic TEMPO is included specifically for the improvement of fouling release, PEG was also included as a hydrophilic component to build a coating that also performs successfully as a more broadly effective antifouling material. The key to the utility of TEMPO depends on its presence at the foulant-coating interface; therefore, PEG was coattached to the same backbone so that both chemistries could also be successfully delivered to the surface in an aqueous environment. Through the combined action of TEMPO, PEG, and PDMS, these coatings should both resist fouling and enhance fouling release. Surfaces were constructed on an elastomeric tie layer and characterized for wettability, surface roughness, and composition by captive bubble contact angle goniometry, laser confocal profilometry, attenuated total reflectance-Fourier transform infrared (ATR-FTIR) spectroscopy, and X-ray photoelectron spectroscopy (XPS) and tested

against a suite of model fouling organisms to correlate surface properties with the antifouling and fouling-release perform-

#### **MATERIALS AND METHODS**

All chemicals purchased from Sigma Aldrich and solvents from VWR were used as received unless otherwise specified. Hexamethylcyclotrisiloxane (D3) and 1,3,5-trivinyl-1,3,5-trimethylcyclotrisiloxane (V3) were purchased from Gelest, Inc. 4-Amino TEMPO was purchased from AK Scientific. Anhydrous ethanol was purchased from Fisher Scientific. Anhydrous N<sub>1</sub>N-dimethylformamide (DMF) was purchased from Alpha Aesar. Benzene was stirred over n-butyl lithium and diphenylethylene, distilled, and freeze-pump-thawed to degas. Styrene was dried over calcium hydride, distilled, and freezepump-thawed to degas. D3 was dissolved in benzene and stirred over calcium hydride for 24 h, at which point a living anionic styrene polymer was added and allowed to stir until the orange color had completely disappeared. The benzene was subsequently distilled, the D3 sublimed, and then, the solution was freeze-pump-thawed to degas. Solution concentration was determined by NMR. Tetrahydrofuran (THF) was stirred over calcium hydride and distilled into a flask containing sodium and benzophenone, which was stirred for at least three days. The THF was subsequently distilled and freezepump-thawed to degas. V3 was stirred over calcium hydride, distilled, and freeze-pump-thawed to degas. Tosyl chloride was dissolved with ether and washed with 1 M NaOH then crystallized by cooling. Glass slides were purchased from Fisher Scientific. Polystyrene-bpoly(ethylene-r-butylene)-b-polystyrene (SEBS, MD6945) and maleic anhydride-grafted SEBS (MA-SEBS, FG1901X) were generously provided by Kraton.

Characterization. Nuclear magnetic resonance <sup>1</sup>H spectra for small-molecule synthesis were recorded on a Varian Gemini 400 MHz and for quantitative polymer spectra on a Bruker INOVA 500 MHz NMR instrument. Gel permeation chromatograms were obtained on a Waters ambient temperature GPC with a Waters 1515 isocratic HPLC pump equipped with both a Waters 2414 differential refractive index detector and a Waters 2489 UV-Vis detector. Samples were eluted at 40 °C. The instrument was calibrated using narrow dispersity polystyrene standards. Attenuated total reflectance-Fourier transform infrared spectra were acquired on a Bruker Vertex 80v vacuum FTIR system. Measurements were made under vacuum in ATR mode using a diamond crystal and recorded using a DTGS detector at room temperature for both bulk and coated samples. Electron paramagnetic resonance (EPR) spectra were acquired using a Bruker EMX X-band CW-EPR spectrometer. Stock solutions were prepared in THF to achieve a radical content of 1 mM. All spectra were double integrated and compared to a 1 mM standard prepared with 4-amino TEMPO to calculate percent radical attachment to the polymer backbone. Surface roughness values and surface images were acquired using a noncontact confocal Keyence VK-X260 laser scanning profilometer. For each coating, average roughness values were calculated from an area of 1.4 mm<sup>2</sup> using three replicate measurements taken over the sample surfaces. Captive bubble contact angle goniometry measurements were taken using an NRL contact angle goniometer (Ramé-Hart model 100-00). An in-house-made sample holder was used to suspend an inverted sample in deionized water. An air bubble was produced using a 22-gauge stainless steel needle and trapped on the underside of the suspended sample. For each coating, a total of five replicate measurements were taken over the surface of the sample and averaged. Contact angles are reported as Young contact angles after correction for roughness using the Wenzel relation and roughness ratios determined from profilometry.<sup>56</sup> X-ray photoelectron spectroscopy measurements were performed on a Surface Science Instruments SSX-100 using a monochromatic Al KlphaX-ray source at 1486.6 eV at pressures below 10<sup>-8</sup> Torr. An electron flood gun was used for surface charge neutralization. Both survey and high-sensitivity spectra were recorded with a pass energy of 150 eV. Spectra were obtained at a 55 degree take-off angle. Samples were

analyzed both as-cast and after soaking in deionized water for 72 h. Spectra were analyzed using CasaXPS v. 2.3.17PR1.1 software.

Polymer Synthesis. PS-PDMS backbones were prepared according to a previously reported method as detailed in the Supporting Information.<sup>52</sup>

Backbone Modification. Thiol-Ene Click. In a typical reaction, a polymer and DMPA (0.2 mol, with respect to polymer vinyl groups) were dissolved in DCM, to which PEG thiol, NHS thiol, or a mixture of the two (5 mol, with respect to polymer vinyl groups) were added. The solution was degassed by bubbling with nitrogen for 15 min, and then, the reaction vessel was exposed to 365 nm UV for 2 h. The polymer was precipitated into methanol, collected by filtration, and then reprecipitated two more times from THF into a 4:1 methanol:water mixture and collected by vacuum filtration. For samples with a higher PEG content, precipitated mixtures were centrifuged to more easily collect the polymer. Samples were dried under vacuum at 55 °C overnight.

TEMPO Incorporation. In a typical reaction, a polymer was dissolved in an inert atmosphere in anhydrous DMF. A solution of triethylamine (5 mol, with respect to polymer NHS groups) and 4amino TEMPO (5 mol, with respect to polymer NHS groups) in anhydrous DMF was added using a cannula. The solution was reacted at 60 °C for 16 h. The polymer was precipitated into water, collected by vacuum filtration, and reprecipitated two more times from THF into water. Samples were dried under vacuum at 55 °C overnight.

Coating Preparation. Coatings were prepared on glass slides using a commercially available elastomeric tie layer of SEBS according to a previously reported method as detailed in the Supporting Information.<sup>5</sup>

Fouling Assays. Balanus improvisus. Barnacle larvae were obtained from broodstocks that are maintained in semicontinuous culture at the Newcastle University. These stocks were originally sourced from the Sven Lovén Centre for Marine Sciences, Tjärnö, Sweden. Adult Balanus improvisus were maintained in a 19 °C recirculating aquarium in brackish conditions, 25 ppt artificial seawater (ASW; Tropic Marin), and fed daily with Artemia sp. and ad libitum with the chlorophyte Tetraselmis suecica. To collect larvae, the adult barnacles were removed from water overnight. On reimmersion, nauplius larvae were released into the water column and collected by attraction to a point light source. Nauplii (approx. 10,000) were transferred into 10 L buckets containing aerated ASW at a salinity of 25 ppt. Nauplii of B. improvisus were initially fed with a 50:50 mixture of T. suecica and Thalassiosira pseudonana with the proportion of T. pseudonana reducing to zero by the third day of culture. The nauplii took between 4-5 days to metamorphose into cyprids, at which point they were collected by filtration and stored in the dark at 6 °C for 3 days.

Three-day-old cyprids of B. improvisus were used in settlement experiments. Six replicate surfaces were placed in quadriPERM dishes, and 1 mL of ASW was initially added to each surface as a droplet. The droplets were of sufficient height on all surfaces to allow free movement of the cypris larvae, which were added 20 per drop. Once all surfaces had cyprids applied, the plates were closed and covered in moist tissue paper to minimize evaporation. The assay was then incubated in the dark at 28 °C for 48 h. Numbers of larvae settled at the end of the assay were expressed as a proportion of the total, averaged per surface, and then compared between surfaces.

For removal assays, a further six replicate surfaces were prepared and treated as per the settlement assay above, using approximately 100 three-day-old cyprids of B. improvisus per droplet. After 48 h, the liquid was removed, and the coatings were rinsed briefly in fresh water to remove any unattached cyprids and then immersed for a further 4 days in artificial seawater containing a dilute concentration of T. suecica. After this period, the number of juvenile barnacles on each surface was counted. Slides were then subjected to water-jetting in a calibrated automated waterjet device system at a cylinder pressure of 30 psi and recounted thereafter. 58 The proportion removed in the experiment was thus calculated for each surface type.

Navicula incerta. All coatings were equilibrated in 0.22  $\mu$ m filtered ASW for 72 h prior to testing. Navicula incerta cells were cultured in

F/2 medium contained in 250 mL conical flasks. 59 After 4 days, the cells were in log phase growth. Cells were washed three times in a fresh medium before harvesting and diluted to give a suspension with a chlorophyll content of approximately 0.25  $\mu$ g/mL.

Cells were settled on three replicate coated slides of each sample, in individual quadriPERM dishes containing 10 mL of the suspension, at approx. 20 °C on the laboratory bench. After 2 h, the slides were exposed to 5 min of shaking on an orbital shaker (60 rpm) followed by a submerged wash in seawater to remove cells that had not attached (the immersion process avoided passing the samples through the air-water interface). Samples were fixed in 2.5% glutaraldehyde and air-dried, and the number of cells attached to each surface was counted on each slide using a Leica LAS X image analysis system attached to a Zeiss Axioscope fluorescence microscope. Cells were visualized by autofluorescence of chlorophyll. Counts were made for 30 fields of view (each 0.15 mm<sup>2</sup>) on each slide.

A further three coated slides of each coating were settled with cells of N. incerta as described above. Slides with attached cells were exposed to a shear stress of 30 Pa in a turbulent-flow water channel.  $^{60}$ Samples were fixed, and the number of cells remaining attached was counted as described above.

Ulva linza. All coatings were equilibrated in 0.22  $\mu$ m filtered ASW for 72 h prior to testing. Zoospores were obtained from mature plants of *Ulva linza* by the standard method. 61 A 10 mL suspension of zoospores (1  $\times$  10<sup>6</sup> spores/mL) was added to individual compartments of quadriPERM dishes containing the samples. After 45 min in darkness, at approx. 20 °C, the slides were washed by moving them backward and forward 10 times through a beaker of ASW to remove unsettled (i.e., swimming) spores. Attached spores were fixed using 2.5% glutaraldehyde in ASW. The number of zoospores attached to the surface was counted on each of the three replicate slides using a Leica LAS X image analysis system attached to an epifluorescence microscope. Spores were visualized by autofluorescence of chlorophyll. Counts were made for 30 fields of view (each 0.15 mm<sup>2</sup>) on

Spores were allowed to settle and attach to the coatings for 45 min and then washed as described above. The spores were cultured using a supplemented seawater medium for 6 days to produce sporelings (young plants) on six replicate slides of each treatment.<sup>62</sup> The sporeling growth medium was refreshed every 48 h. Sporeling biomass was determined in situ by measuring the fluorescence of the chlorophyll contained within the sporelings in a Tecan fluorescence plate reader. Using this method, the biomass was quantified in terms of relative fluorescence units (RFU). The RFU value for each sample is the mean of 70-point fluorescence readings taken from the central portion. The sporeling growth data are expressed as the mean RFU of six replicate slides.

Removal of sporelings was assessed using a shear stress of 90 Pa in a turbulent flow cell.<sup>63</sup> Biomass remaining was determined using the fluorescence plate reader (as above). The percentage removal was calculated from readings taken before and after exposure to the shear

Statistical Analysis. All biological assays are presented as means with 95% confidence limits. One-way ANOVA was performed to identify statistically significant differences between groups (p < 0.05) followed by a post hoc pairwise Tukey comparison test for data presented in the main text to compare individual means and identify which are statistically different from one another.<sup>64</sup> For assays reported as a percentage (B. improvisus settlement and removal and removal of N. incerta and U. linza), statistical tests were performed on the arcsine transform of fractional data.

# **RESULTS AND DISCUSSION**

Material and Coating Preparation. Coatings were based on a previously studied system using a polystyrene-bpoly(dimethylsiloxane-r-vinylmethysiloxane) (PS-PDMS) block copolymer. 52-55 When functionalized with sequencecontrolled amphiphilic side groups, this system has shown promising performance against soft fouling species Ulva linza

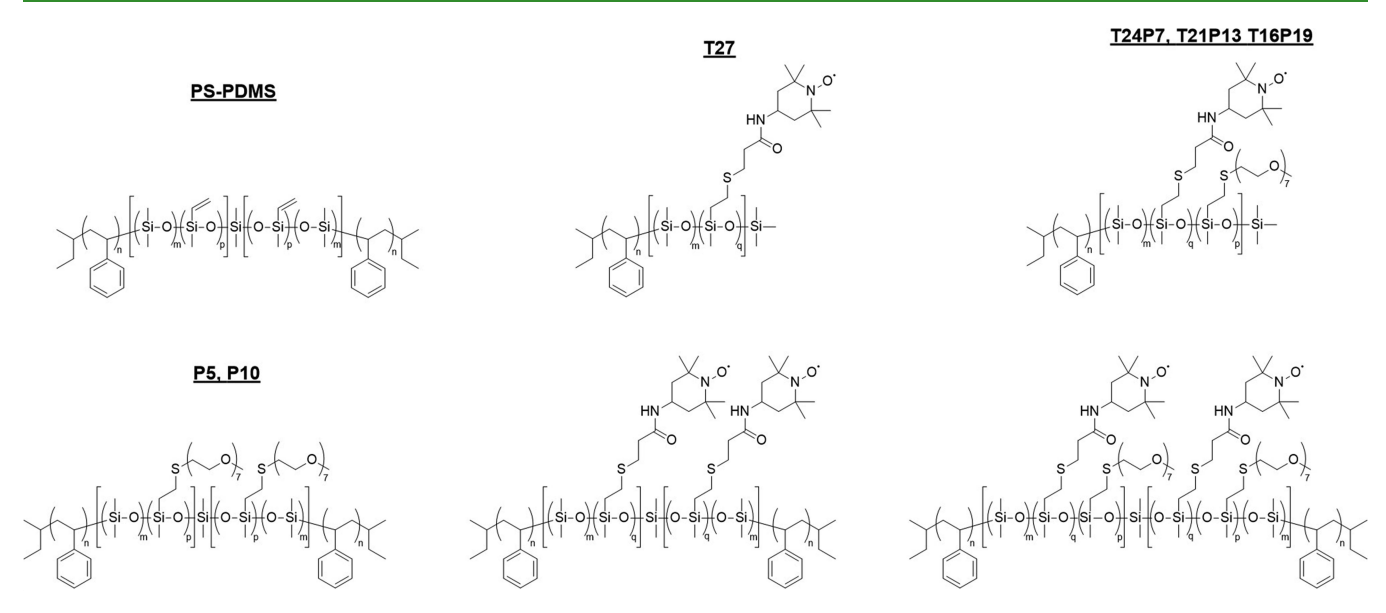


Figure 1. Structures of the unfunctionalized PS-PDMS, PEG-functionalized PS-PDMS, TEMPO-functionalized PS-PDMS, and TEMPO-PEG-cofunctionalized PS-PDMS backbones used in coating construction.

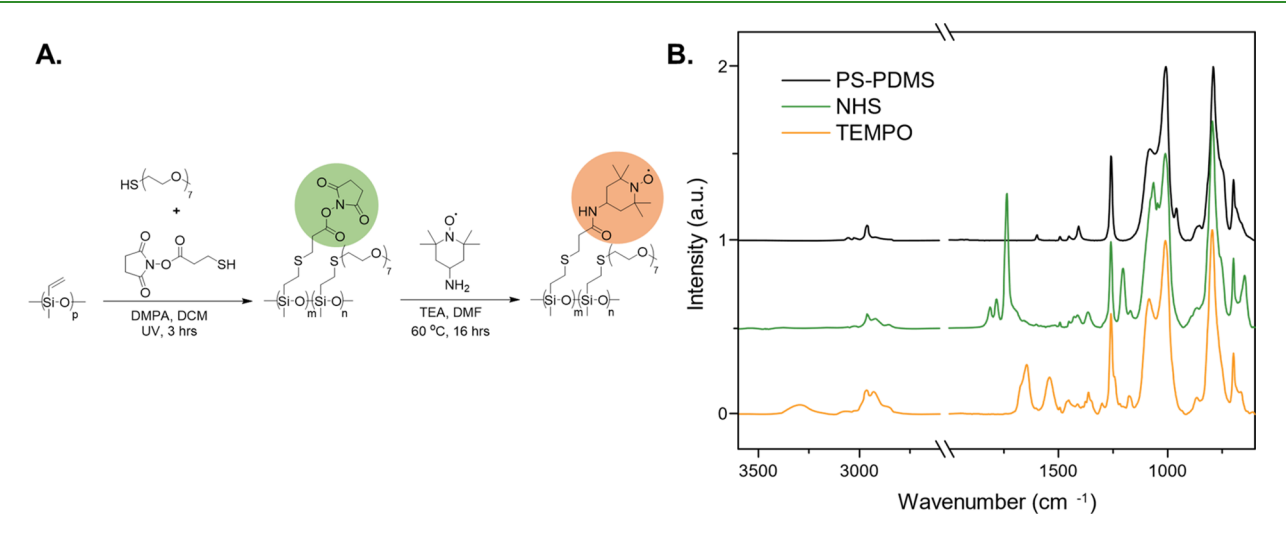


Figure 2. Modification of the silicone backbone block cofunctionalized with TEMPO and PEG used in the study of PS-PDMS TEMPO-PEG-cofunctionalized coatings. (A) Conditions used for the stepwise attachment of TEMPO nitroxide. (B) FTIR data showing the appearance, and subsequent disappearance, of NHS characteristic peaks and the appearance of amide I and II peaks indicative of the amide used to attach TEMPO.

Table 1. Polymer Functionalization and Corresponding Sample Codes for PS-PDMS TEMPO-PEG-Cofunctionalized Coatings

code	T27		T24P7		T21P13		T16P19		P5	P10
backbone structure	diblock	triblock	diblock	triblock	diblock	triblock	diblock	triblock	triblock	triblock
mol % NHS with respect to the siloxane block $^{a}$	37.5	37.7	32.2	31.6	25.8	27.5	19.8	19.1		
mol % TEMPO with respect to the siloxane block $^b$	27.2	26.4	23.7	24.0	19.7	22.2	16.7	16.1		
mol % PEG with respect to the siloxane block $^{a}$			6.6	8.0	13.4	13.2	19.4	17.7	5.0	10.6
coating avg. mol % TEMPO with respect to the siloxane block $^c$	26.8		23.9		21.0		16.4			
coating avg. mol % PEG with respect to the			7.3		13.3		18.6		5.0	10.6

"With respect to the PDMS block determined by H¹ NMR. "With respect to the PDMS block determined by EPR. "Coatings consist of a 50/50 mixture of the diblock and triblock. The coating content was calculated by averaging the diblock and triblock value.

and *Navicula incerta*. <sup>52–55</sup> Previous studies have shown that coatings composed of a mixture of amphiphilic diblock and triblock scaffolds promoted higher removal of *U. linza* than the

triblock copolymer alone, even though all materials had the same relative content of PS, PDMS, and PEG.<sup>65</sup> For this reason, a blend of the two architectures was used in this study.

Backbones were constructed with PS blocks of 6–8k and PDMS blocks of 30–35k; triblocks were generated by the coupling of two identical diblocks resulting in PDMS block lengths of 60–70k.

Polymer modification was done using thiol-ene click chemistry to attach PEG and TEMPO to pendent vinyl groups on the PDMS block (Figure 1). Due to the radical nature of the thiol-ene reaction, a two-step attachment scheme was employed to avoid quenching by the TEMPO radical (Figure 2).<sup>51</sup> A thiol-bearing N-hydroxysuccinimide (NHS) ester was synthesized and attached to the PDMS block at the vinyl functionalities. This chemistry allowed for subsequent attachment of the TEMPO moiety using a commercially available, amine-bearing, TEMPO to form an amide. To achieve amphiphilic surfaces, the stable radical was also coattached to the same backbones with a seven repeat unit PEG (350 g/mol), which was done simultaneously to the attachment of the activated NHS ester. It was found that the reactivity of the PEG and NHS thiols differs, resulting in lower ratios of PEG attachment compared to the feed ratio used, as detailed in the Supporting Information. This was thought to occur because of the larger size and more hydrophilic nature of the PEG group compared to the NHS counterpart. Details of prepared coatings, and their corresponding sample codes, are in Table 1. Coatings P5 and P10 were prepared using only triblock backbones, as the diblock backbones showed significant solubility in water and could not be precipitated effectively.

Polymer functionalization was followed using a combination of NMR, FTIR, and EPR. Figure 2 shows the sequential modification monitored by FTIR. Peaks at 1752, 1784, and 1813 cm<sup>-1</sup> are characteristic of the NHS ester group. Their subsequent disappearance and the appearance of peaks at 1641 and 1541 cm<sup>-1</sup>, the amide I and II peaks, indicate the attachment of TEMPO. The peak at 1362 cm<sup>-1</sup> is characteristic of the nitroxide N-O. functionality. 66 EPR analysis further confirms the presence of the nitroxide radicals on the polymer backbone, and quantification of the radical content was done by solution-state EPR. EPR spectra also give a qualitative indication of the distribution and spacing of the nitroxide along the backbone. Changes in the line shape are related to the interaction of radicals on the backbone. Typically, free nitroxides display a distinct triplet line shape, attributed to the rapid translational and rotational motion of the radicals, which limit the opportunities for spin exchange.<sup>67</sup> When the radicals are tethered in proximity to other radical units, translational and rotational motions are limited, leading to larger electron dipole-dipole interactions and increased spin exchange frequency. This results in broadening of the triplet as the signal coalesces into a singlet.<sup>67,68</sup> Evidence of this is shown in Figure 3: higher loadings of TEMPO trend toward line shapes resembling a broad singlet rather than a triplet because of restricted motion of radicals in close proximity to one another attached to the polymer backbone.

Coatings were constructed using a previously devised architecture that utilizes a tie layer of a commercially available thermoplastic elastomer. <sup>57,69,70</sup> Glass slides were functionalized with an amino silane, which was then reacted with a maleic anhydride-functionalized elastomer. This elastomer, polystyrene-*b*-poly(ethylene-*r*-butylene)-*b*-polystyrene (SEBS), was then successively spin-coated to build up a thick layer (~1 mm), on top of which the PS-PDMS was deposited by spray-coating. Spray-coating was used for this deposition to more

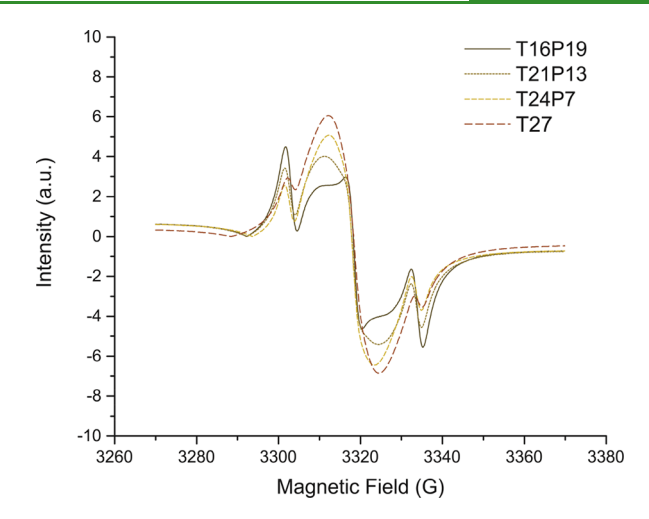


**Figure 3.** EPR spectra of TEMPO and TEMPO-PEG modified backbones in the study of PS-PDMS TEMPO-PEG-cofunctionalized coatings.

directly mimic the methods used for marine paint application. The SEBS acted as a tie layer ensuring stable attachment of the functionalized PS-PDMS to the substrate through physical cross-links between the styrene end blocks of the copolymers. The tie layer also provided more consistent bulk mechanical properties between coating types, which is known to be important in fouling-release performance. This combination allows for evaluation of coating surface chemistry more directly and removes the variable of mechanical properties from the overall analysis. Using a commercially available material allowed the deposition of a thick coating, better for fouling release, and required less of the synthesized PS-PDMS material.

Coating Characterization. The wettability of the system was probed through captive bubble contact angle measurements, as shown in Figure 4. This method was carried out with the sample fully immersed in water, and the contact angle was measured between a trapped air bubble in contact with the surface. The measurement is analogous to a typical water contact angle measurement but allows for the measurement to be performed in an aqueous environment, similar to the

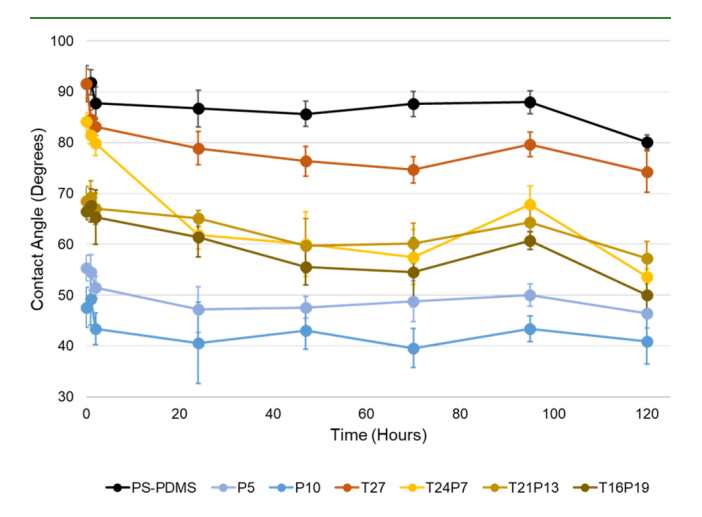


**Figure 4.** Captive bubble advancing contact angles over a 4-day period of PS-PDMS TEMPO-PEG-cofunctionalized coatings. Error bars show standard deviation.

ultimate operating environment of the coating.<sup>73</sup> Modification with either PEG or TEMPO lowered the contact angle compared to the unfunctionalized control, with greater amounts of PEG leading to lower initial contact angles. PEG-functionalized coatings showed lower contact angles than their equivalent TEMPO-PEG counterparts; coating T16P19 exhibited a contact angle at least 5° greater than coating P5 despite having an almost four times greater loading of PEG, indicating that the presence of the TEMPO mitigates the hydrophilic action of PEG. This is not unexpected; TEMPO materials have been shown to have a surface energy of 30.12 mN/m and so are more hydrophobic than PEG. 74 The PEG coatings also reached equilibration more quickly, with little change after 24 h, whereas the TEMPO coatings took closer to 72 h on average to reach equilibrium. Competition between TEMPO and PEG at the surface is the likely cause of the longer equilibration times and ultimately higher contact angle values.

ATR-FTIR analysis was carried out to probe the chemical functionalities at the surface. Evidence of the presence of TEMPO at the surface (Figure 5) can be seen with observation

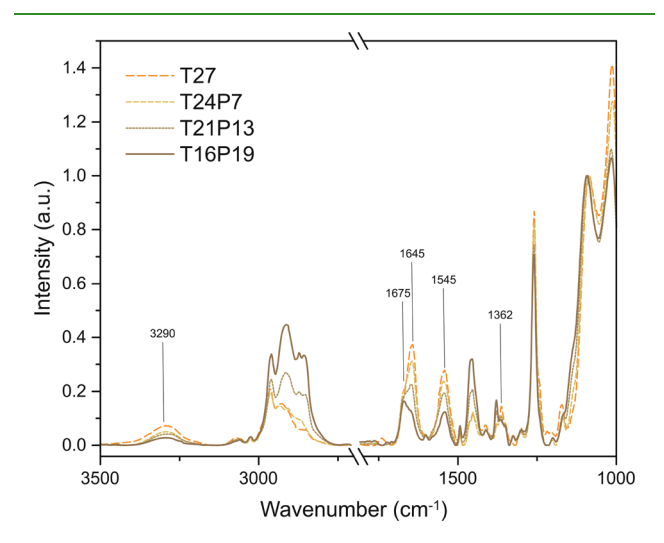


**Figure 5.** ATR-FTIR spectra of PS-PDMS TEMPO-functionalized and TEMPO-PEG-cofunctionalized coating surfaces (a.u. = arbitrary units).

of a characteristic N-O peak at 1362 cm<sup>-1</sup>, 66 which shows an increase in intensity with higher TEMPO attachment to the polymer backbone. Peaks at 1645 and 1545 cm<sup>-1</sup> correspond to the amide I and amide II peaks, respectively, and are characteristic of the amide used for TEMPO attachment. There was a significant reduction in the intensity of these two peaks when the percentage attachment of TEMPO to the backbone was reduced. This change was also observed in the N-H stretch at 3290 cm<sup>-1</sup>, which is also associated with the amide functionality, and shows decreasing intensity with a reduction of TEMPO attached to the backbone. An interesting trend was related to the presence of a peak at 1675 cm<sup>-1</sup> which became more obvious with the increasing PEG attachment to the backbone. This can be explained by a disruption in hydrogen bonding to the carbonyl oxygen and a subsequent shift of the carbonyl peak to a higher wavenumber.<sup>75</sup> This trend follows the reduction in TEMPO attachment to the backbone, indicating that the amide groups were more distantly spaced along the backbone and could no longer hydrogen-bond with one another. The N-H stretch did not appear as a second peak at a higher wavenumber, which would be expected if the amide NH no longer participated in a hydrogen bond. 76 This likely resulted from the N-H hydrogen bonding with the PEG functionalities instead.

Coatings were analyzed by XPS in both the as-deposited state and after being immersed in water for 96 h. Highsensitivity N 1s scans showed a signal both before and after immersion, as exemplified by T24P7 spectra in Figure 6, indicating the presence of the nitroxide at the surface in both aqueous and ambient conditions. Although XPS measurements are done under high vacuum, surface rearrangement was shown to occur over days by captive bubble contact angle measurements, so the presence of the nitrogen signal is likely indicative of the presence of the nitroxide at the coating surface, even in water. All coatings showed less nitrogen content at the surface than theoretically expected, which was further decreased upon exposure to water, likely due to the competition of the nitroxide with both PDMS and PEG for surface dominance. Coatings T24P7, T21P13, and T16P19 showed decreasing nitrogen at the surface with less nitroxide attached to the backbone. Interestingly, coating T27 showed a lower percentage of nitrogen at the surface (1.47%) than coating T24P7 (3.24%) in the as-deposited state, even though

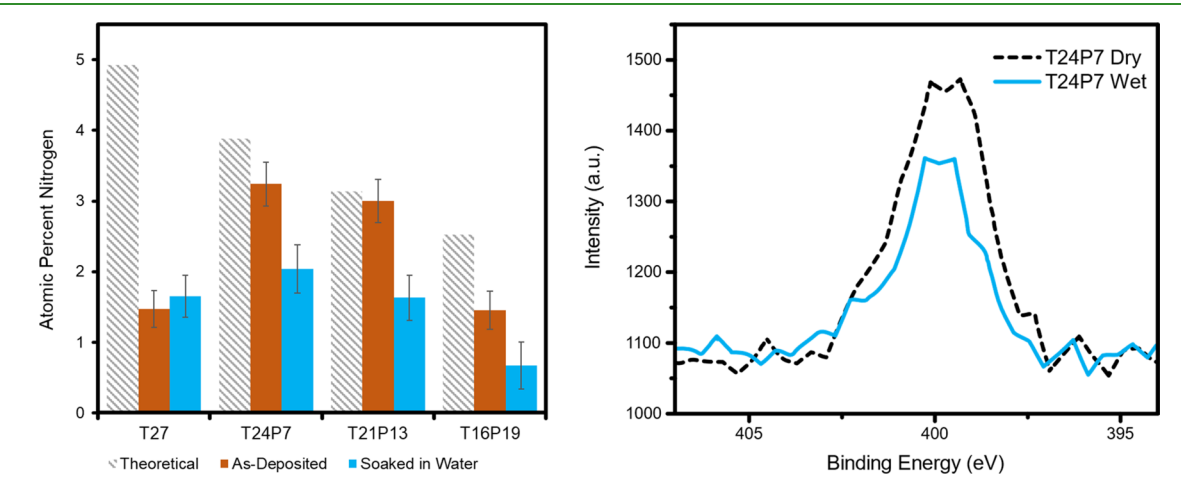


Figure 6. (Left) Nitrogen composition at the surface of PS-PDMS TEMPO-functionalized and TEMPO-PEG-cofunctionalized coatings and (right) XPS N 1s scans of T24P7 showing the signal change after immersion in water for 96 h. Error bars show standard deviation.

it had a higher nitroxide content. This could be a result of the presence of PEG on the same backbone as the TEMPO, which may cause the backbone to adopt a conformation that drives more of the nitroxide to the surface in an effort to bury the PEG. The discrepancy with the IR results, which showed T27 as having the highest intensity for both the TEMPO N-O peak and the amide I and II peaks, is likely a result of the acquisition conditions required for the two measurement techniques. ATR-FTIR is more indicative of the bulk coating than XPS since it has a sampling depth of about a micrometer, which is far greater than the 10 or so nanometers of XPS. All coatings showed less carbon than would theoretically be expected, while the percentage of silicon and oxygen was greater, as detailed in the Supporting Information. This reflected the surface dominance of the PDMS block that outcompeted the styrene block to populate the surface because of its low surface energy (20.4 mN/m).7

Surface roughness of the coatings was measured by laser profilometry. Figure 7 and Table 2 show that including

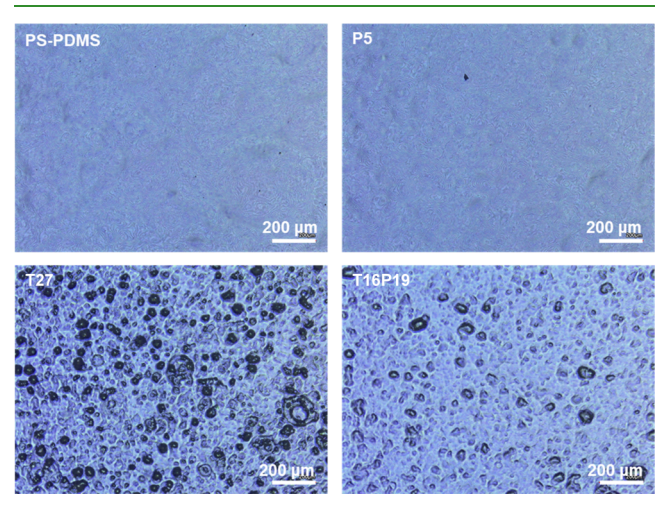


Figure 7. Surface morphology of PS-PDMS TEMPO-functionalized and TEMPO-PEG-cofunctionalized coating surfaces. TEMPO-containing coatings (T27 and T16P19) all exhibit significantly rougher surfaces than PS-PDMS and P5.

Table 2. Summary of Surface Features for PS-PDMS TEMPO-PEG-Cofunctionalized Coatings, Determined by Laser Profilometry

	$R_a (\mu m)^a$	$R_{\rm q} (\mu \rm m)^b$	$R_{z} (\mu m)^{c}$
PS-PDMS	$0.935 \pm 0.176$	$1.222 \pm 0.224$	$13.050 \pm 2.331$
P5	$0.832 \pm 0.127$	$1.107 \pm 0.192$	$14.100 \pm 4.731$
P10	$0.959 \pm 0.075$	$1.259 \pm 0.094$	$13.717 \pm 1.134$
T27	$3.386 \pm 0.202$	$7.405 \pm 0.419$	$152.546 \pm 11.520$
T24P7	$2.019 \pm 0.060$	$2.573 \pm 0.135$	$64.434 \pm 25.611$
T21P13	$2.186 \pm 0.242$	$2.920 \pm 0.553$	$57.585 \pm 22.357$
T16P19	$2.060 \pm 0.208$	$2.731 \pm 0.221$	$61.910 \pm 38.339$
SEBS	$0.221 \pm 0.033$	$0.286 \pm 0.054$	$2.719 \pm 2.719$

<sup>a</sup>Arithmetic mean roughness. <sup>b</sup>Root-mean-square roughness. <sup>c</sup>Maximum height, sum of the largest peak and largest valley.

TEMPO in the formulation resulted in at least a doubling of roughness compared to PEG or PS-PDMS control coatings. The control and PEG coatings showed arithmetic average  $(R_a)$ roughness values of around 1  $\mu$ m, while all TEMPO-PEG coatings had  $R_a$  values closer to 2  $\mu$ m, and coating T27 had an

 $R_a$  value of almost 3.5  $\mu$ m. This trend was also reflected in the maximum feature heights  $(R_{\gamma})$ , which showed an almost 10fold increase from the maximum height of the unfunctionalized PS-PDMS and PEG coatings (13–14  $\mu$ m) to coating T27 (150 um). Spray-coating contributed somewhat to surface roughness, as evidenced by the increase in roughness between the SEBS underlayer, which was spin-coated, and the unfunctionalized PS-PDMS control, which was spray-coated. However, the increased roughness of TEMPO coatings was likely a result of more limited solubility of the TEMPO-functionalized backbones in the deposition solvent. This accounts for the lower roughness of TEMPO-PEG coatings compared to coating T27, which can be attributed to the PEG increasing the solubility of the polymer.

Barnacle Assays. To evaluate the performance of coatings against hard fouling species, settlement and removal assays using the acorn barnacle Balanus improvisus were conducted, the results of which are presented in Figure 8. Incorporation of TEMPO did not appear to reduce or enhance settlement, with T27 (70.0  $\pm$  9.7% settled cyprids) not performing significantly differently from the unfunctionalized control (58.0  $\pm$  10.7% settled cyprids). Inclusion of PEG greatly improved resistance to settlement in coatings both with and without TEMPO; P5, P10, and T16P19 performed exceptionally well, with no settlement whatsoever, and T21P13 had very low settlement  $(3.3 \pm 3.3\% \text{ settled cyprids})$ . In removal assays using a 30 psi waterjet, functionalization with nitroxide showed promise for improving fouling release. Coating T27 demonstrated almost a 2-fold increase in removal (58.1  $\pm$  5.0% removed) as compared to the unfunctionalized PS-PDMS control (27.0  $\pm$ 4.4% removed). T24P7 was further enhanced with three times greater removal (90.4  $\pm$  9.3%) than that of the control. The very low or complete inhibition of settlement on P5, P10, T21P13, and T16P19 meant that acquisition of removal data was not possible. Notably, there were several metamorphosed juvenile barnacles floating in the medium above coatings T21P13 and T16P19. This would indicate that settlement occurred but that the resulting organisms spontaneously detached from the surface. There was no such evidence of settlement on the two PEG coatings, only the presence of unsettled cyprids swimming above coatings.

These results demonstrate the fouling-release potential of the nitroxide moiety through interference with barnacle adhesion and promotion of fouling release. Coating T27 showed twice the fouling release compared to the unfunctionalized control, while coating T24P7 showed almost three times greater removal. Despite the bulk having a lower loading of nitroxide, T24P7 did show a higher percentage of nitrogen (and therefore nitroxide) at the surface than T27, which may explain its enhanced performance. The XPS analysis showed that there was a lower nitrogen content at the surface for coatings T21P13 and T16P19, and consequently, they would be expected to show lower removal than T24P7. Coatings also showed excellent performance against barnacles in terms of preventing settlement. Despite the nitroxide's structural and electronic similarity to nitric oxide, which has been shown to inhibit larval settlement in the barnacle species Amphibalanus amphitrite, it did not have any influence on settlement, with the performances of T27 and T24P7 being statistically the same as the control.<sup>77</sup> T21P13 and T16P19 were able to inhibit settlement almost completely, similar to the performance of P5 and P10, which indicates that PEG was a major contributing factor to overall antifouling performance against barnacle

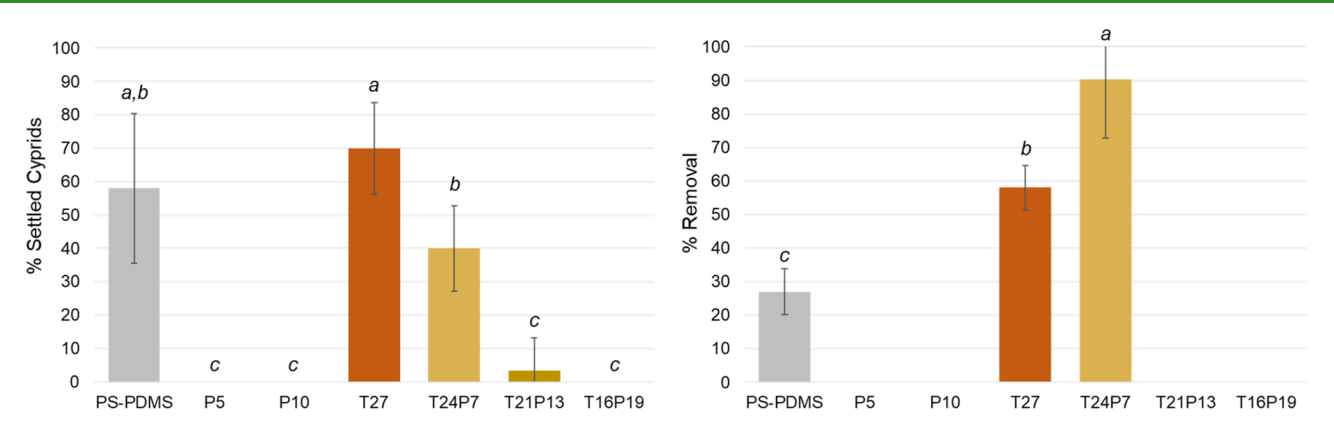


**Figure 8.** Settlement of cyprids of *Balanus improvisus* after 48 h (left) and removal of 6-day-old juveniles (right) following exposure to a 30 psi waterjet. Samples with little to no settlement (P5, P10, T21P13, and T16P19) could not be evaluated for removal. Bars show 95% confidence limits derived from arcsine transformed data for settlement and removal. Values that are significantly different at p < 0.05 from a post hoc pairwise Tukey test are indicated by different labels (a–c). In the case of T21P13 and T16P19, unattached metamorphosed juveniles were observed floating above the coating surfaces, while P5 and P10 only had swimming cyprids.

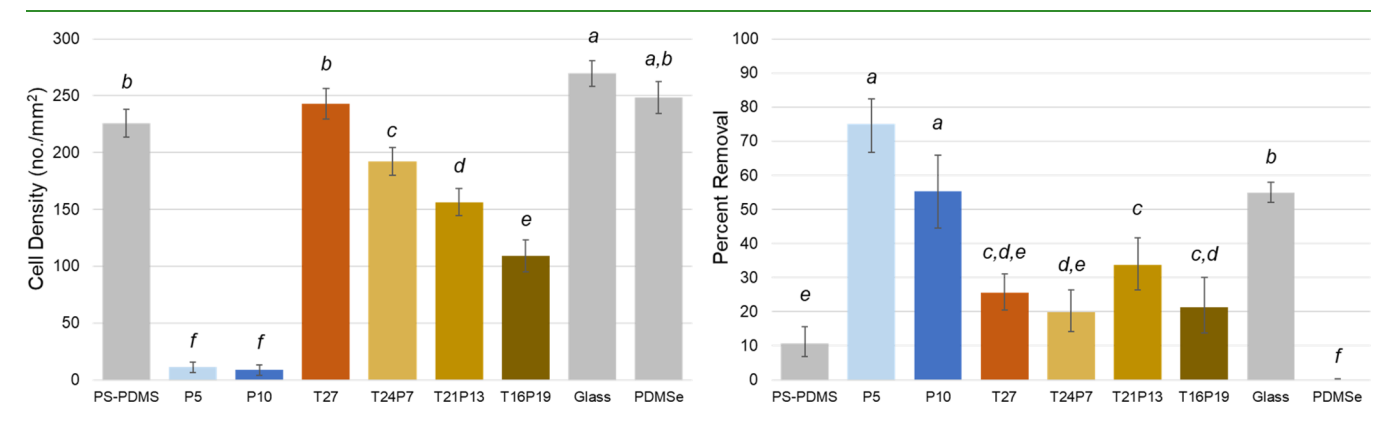


**Figure 9.** Initial attachment density of cells of the diatom *N. incerta* (left) and removal due to exposure to a shear stress of 30 Pa (right). Bars show 95% confidence limits for settlement and 95% confidence limits derived from arcsine transformed data for removal. Values that are significantly different at p < 0.05 from a post hoc pairwise Tukey test are indicated by different labels (a–f).

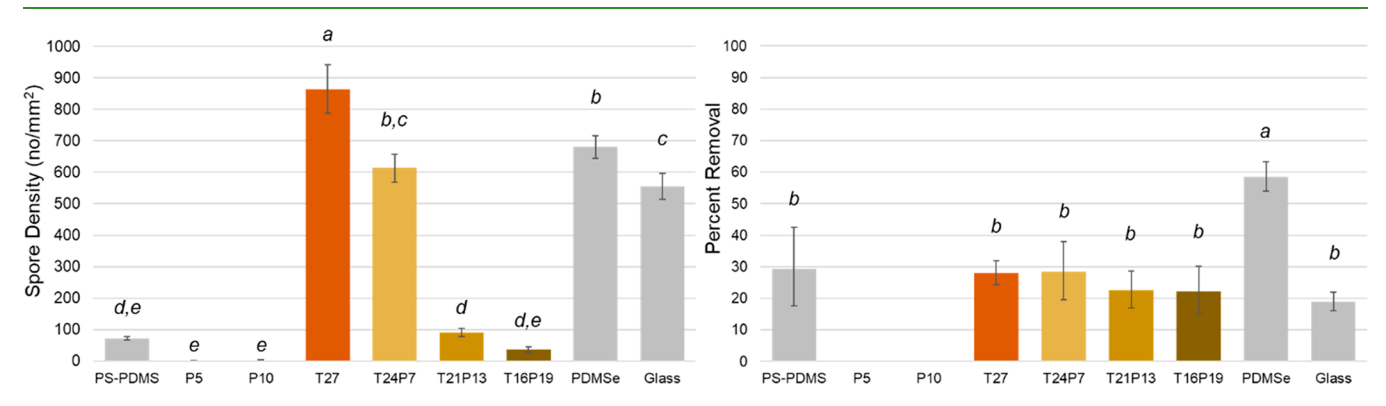


**Figure 10.** Density of attached spores of *U. linza* after 45 min settlement (left) and percent removal of 6-day-old sporelings (young plants) due to a shear stress of 90 Pa in a turbulent-flow water channel (right). Bars show 95% confidence limits for settlement and 95% confidence limits derived from arcsine transformed data for removal. Values that are significantly different at p < 0.05 from a post hoc pairwise Tukey test are indicated by different labels (a–e). Samples with no settlement (P5, P10) could not be evaluated for percent removal.

cyprids. Altogether, these results suggest that fine-tuning the relative composition of TEMPO and PEG may lead to even more effective antifouling and fouling-release characteristics against barnacles.

**Soft Fouling Assays.** The performance against algae was also evaluated using the diatom *N. incerta* and spores of *U. linza*. Against *N. incerta*, functionalization with nitroxide did not improve the antifouling or fouling-release performance. Figure 9 shows that T27 and the control did not differ

significantly in terms of initial attachment density ( $243 \pm 13.4$  and  $225 \pm 12.3$  cells/mm², respectively). Coatings P5 and P10 were the most successful at preventing settlement, with both maintaining settlement densities at least 20 times less than the control. The addition of PEG to the nitroxide coatings reduced settlement relative to the control and T27, with lower settlement correlating with greater PEG loading. The improved antifouling performance of those coatings can be assumed to derive solely from the inclusion of PEG, but even at the highest

loading of PEG, performance was still worse than either P5 or P10. In removal assays against *N. incerta* utilizing a 30 Pa shear stress water channel, P5 and P10 coatings showed superior performance with removal from both coatings above 50%. The TEMPO coatings all performed similar to or worse than the control, with no improvement in removal with an increased loading of PEG. This indicates that the incorporation of TEMPO does not reduce the adhesion of *N. incerta* cells.

The coatings were prepared using a blend of both diblock and triblock backbones. In the initial preparation of these coatings, it was found that the diblock backbones functionalized with only PEG showed significant solubility in water. During purification, these materials could not be precipitated, so coatings P5 and P10 were composed of only triblock materials. Backbones functionalized with both PEG and TEMPO, even at the highest PEG functionalization, showed no solubility issues, so both the diblock and triblock were used in coating preparation. After the six-day growth period for U. linza removal assays, however, T16P19 and T21P13 exhibited delamination from the SEBS underlayer. This was likely caused by the slow solubilization of the diblock backbone, supported by the fact that P5 and P10, containing only the triblock backbone, showed no issues with coating stability even when exposed to a shear stress of 20 Pa waterjet (as detailed in Supporting Information Figures S10-12). Coatings were reprepared using only the triblock backbone for U. linza assays. These coatings showed no instability even in removal experiments using shear stresses up to 90 Pa.

The coatings in *U. linza* assays exhibited similar trends to those used against N. incerta (Figure 10) with the exception that initial settlement of *U. linza* was considerably higher on the T27 (863.8  $\pm$  77.1 spores/mm<sup>2</sup>) and T24P7 (612.8  $\pm$  44.9 spores/mm<sup>2</sup>) coatings than on the unfunctionalized PS-PDMS control (72.3  $\pm$  5.7 spores/mm<sup>2</sup>). This was mitigated by the incorporation of PEG, as shown by the trend of decreasing settlement density with increasing incorporation of PEG with coating T16P19, having about 50% lower settlement (36.3 ± 8.8 spores/mm<sup>2</sup>) than the PS-PDMS control. P5 and P10 had the best performance, maintaining close to zero settled spores. After 6 days of culture, the relative trends of growth resembled those of the initial settlement, with the TEMPO-containing coatings still having the highest biomass levels (Figure S9). However, the relative growth on the control was significantly increased compared to T27, with only two times the biomass on T27, down from 10 times in settlement assays. Removal assays indicated that the incorporation of TEMPO did not enhance the release of sporelings of U. linza. As was the case for N. incerta, incorporation of increasing amounts of PEG did not have a strong effect on performance, with all the TEMPO coatings performing similarly. Settlement and growth were so low on the PEG coatings that removal experiments could not be performed, although previous studies have shown that these coatings tend to perform very well against *U. linza.* 65

While TEMPO plays a beneficial role in barnacle fouling release, it did not appear to otherwise impart any benefits against the soft fouling algae. As a hydrophobic component, it neither increased nor decreased settlement of *N. incerta*, but it increased the settlement of *U. linza* by almost tenfold. For both fouling species, the incorporation of PEG helped to mitigate settlement, although the improvement with an increased loading of PEG was more pronounced for *U. linza*. Despite having higher loadings of PEG, both T21P13 and T16P19 showed higher settlement than P5 or P10. This may in part be

attributable to the greater wettability of P5 and P10, for which contact angles were significantly lower. TP coatings had higher surface roughness, 78 which is known to increase settlement for U. linza spores, but there may be some other favorable interactions at play, unrelated to wettability or surface morphology. The oxidized form of the nitroxide (oxoammonium) is a protonated species with a positive charge, so if overoxidation of the surface occurred, it could attract the negatively charged *U. linza* spore body. <sup>79</sup> An additional factor could be that a primary amide was used to attach the nitroxide to the backbone. In previous studies of this system that compared the performance of side groups with and without hydrogen bond donors, the presence of the hydrogen bond donor led to both higher settlement and lower removal of U. linza. 54,55 Use of an alternate linkage could improve performance.

For both algal species, the fouling-release performance was generally poor, with removal values for all TEMPO coatings not better than the control. Roughness is likely a large contributing factor to this performance. U. linza spores are around 4–5  $\mu$ m in diameter, and N. incerta diatoms are 13  $\mu$ m in length.<sup>80,81</sup> With maximum feature heights between 50 and 150  $\mu$ m, the TEMPO coatings may offer protection from hydrodynamic forces, which could explain why the TEMPO coatings had a performance similar to or worse than the PS-PDMS control, despite having lower contact angle values. Smoother surfaces, resembling those of the control, P5, and P10, could greatly improve performance of the TEMPOcontaining materials. Although nitroxides have been shown to reduce the formation and proliferation of bacterial biofilms, 39-42 these coatings performed considerably better against barnacles than diatoms. Specifically, nitric oxide has been shown to act as a signaling molecule in some species of diatoms, limiting cell growth and reducing adhesion, 82,83 but those effects were not seen in the assays against N. incerta. One reason for this could be that diatom assays were of short duration, with cells only in contact with the surface for 2 h before removal experiments were performed, and this may not have provided enough time for the nitroxide to have an effect. A longer incubation time using diatom biofilms rather than single cells might allow any effects on diatom behavior to become evident.

# CONCLUSIONS

In this study, PS-PDMS block copolymers were functionalized with a nonpolar stable radical nitroxide and PEG to create antioxidant, amphiphilic surfaces for use as marine antifouling and fouling-release coatings. Many marine foulers use oxidatively cross-linked cements, so incorporation of a stable radical was explored to probe disruption of cementation to reduce adhesion and improve fouling release. Coatings were evaluated for their performance against a barnacle species, as well as a diatom and spores of a green alga, to ensure that the antifouling and fouling-release properties of the amphiphilic siloxane coatings were tested against a range of relevant organisms.

Performance against the barnacles was promising. Incorporation of TEMPO alone led to a 2-fold increase in removal compared to the unfunctionalized control, while a combination of TEMPO and PEG gave close to 90% removal. The presence of detached metamorphosed juvenile barnacles above TEMPO coatings bolsters the hypothesis that the nitroxide works to limit adhesive interactions at the surface. Coatings also

performed extremely well as antifouling surfaces against barnacles, with two of the TEMPO compositions completely inhibiting barnacle settlement. Performance against soft fouling species was not as pronounced. TEMPO coatings with the highest loading of PEG were able to reduce settlement by 50% compared to the control for both algal species, but the incorporation of TEMPO led to higher settlement of spores of U. linza. No benefit was seen in fouling release with incorporation of TEMPO, but the higher surface roughness of the TEMPO coatings may have contributed to this performance. Improvement of surface roughness and optimization of TEMPO and PEG ratios could lead to a more broad-spectrum antifouling and fouling-release coating.

For barnacles, a combination of TEMPO and PEG on PDMS produces a surface where settlement and removal appear to be controlled by different components of the coating. The presence of PEG is essential in maintaining antifouling activity as evidenced by the performance of T27, but there is significant improvement of fouling release of barnacles with the incorporation of TEMPO. Overall, these results offer a promising new avenue of research for construction of fouling-release coatings for hard fouling organisms but also highlight the importance of balancing hydrophilic and hydrophobic contents to maintain a broad-spectrum efficacy against a range of fouling species.

# ASSOCIATED CONTENT

# Supporting Information

The Supporting Information is available free of charge at https://pubs.acs.org/doi/10.1021/acsami.1c05266.

Detailed synthetic procedures for block copolymers and small molecules, GPC and <sup>1</sup>H NMR characterization data for the block copolymer and its derivatives, EPR of the TEMPO standard, detailed coating preparation procedures, roughness ratios calculated from profilometry, complete XPS surface compositions, and additional fouling assay data (PDF)

# AUTHOR INFORMATION

#### **Corresponding Author**

Christopher K. Ober - Department of Materials Science and Engineering, Cornell University, Ithaca, New York 14853, United States; orcid.org/0000-0002-3805-3314; Email: cko3@cornell.edu

Amanda Leonardi – Department of Chemistry and Chemical Biology, Cornell University, Ithaca, New York 14853, United States

Aria C. Zhang - Department of Materials Science and Engineering, Cornell University, Ithaca, New York 14853, United States

Nilay Düzen - Department of Materials Science and Engineering, Cornell University, Ithaca, New York 14853, United States

Nick Aldred - School of Life Sciences, University of Essex, Colchester CO4 3SQ, United Kingdom; School of Natural and Environmental Sciences, Newcastle University, Newcastle upon Tyne NE1 7RU, United Kingdom

John A. Finlay - School of Natural and Environmental Sciences, Newcastle University, Newcastle upon Tyne NE1 7RU, United Kingdom

Jessica L. Clarke - School of Natural and Environmental Sciences, Newcastle University, Newcastle upon Tyne NE1 7RU, United Kingdom

Anthony S. Clare - School of Natural and Environmental Sciences, Newcastle University, Newcastle upon Tyne NE1 7RU, United Kingdom; orcid.org/0000-0002-7692-9583

Rachel A. Segalman - Department of Chemical Engineering, University of California Santa Barbara, Santa Barbara, California 93110, United States; o orcid.org/0000-0002-4292-5103

Complete contact information is available at: https://pubs.acs.org/10.1021/acsami.1c05266

#### **Author Contributions**

The manuscript was written through contributions of all authors. All authors have given approval to the final version of the manuscript.

#### Notes

The authors declare no competing financial interest.

# ACKNOWLEDGMENTS

This research was supported by the Office of Naval research awards N00014-16-1-2960, N00014-16-1-2988, and N00014-16-1-3125. This work made use of the Cornell Center for Materials Research Shared Facilities, which are supported through the NSF MRSEC program (DMR-1719875). This work made use of the Cornell University NMR Facility, which is supported, in part, by the NSF through MRI award CHE-1531632. This work also made use of the shared facilities of the National Biomedical Center for Advanced Electron Spin Resonance Technology, which is supported by the National Institute of General Medical Sciences of the National Institutes of Health (P41GM103521).

### REFERENCES

- (1) Lindholdt, A.; Dam-Johansen, K.; Olsen, S. M.; Yebra, D. M.; Kiil, S. Effects of Biofouling Development on Drag Forces of Hull Coatings for Ocean-Going Ships: A Review. J. Coatings Technol. Res. 2015, 12, 415-444.
- (2) Schultz, M. P.; Walker, J. M.; Steppe, C. N.; Flack, K. A. Impact of Diatomaceous Biofilms on the Frictional Drag of Fouling-Release Coatings. Biofouling 2015, 31, 759-773.
- (3) Schultz, M. P.; Bendick, J. A.; Holm, E. R.; Hertel, W. M. Economic Impact of Biofouling on a Naval Surface Ship. Biofouling 2011, 27, 87-98.
- (4) Donnelly, B.; Bedwell, I.; Dimas, J.; Scardino, A.; Tang, Y.; Sammut, K. Effects of Various Antifouling Coatings and Fouling on Marine Sonar Performance. Polymers (Basel). 2019, 11, 663.
- (5) Hewitt, C. L.; Gollasch, S.; Minchin, D. The Vessel as a Vector -Biofouling, Ballast Water and Sediments. In Biological Invasions in Marine Ecosystems; pp. 117-131.
- (6) Brooks, S. J.; Waldock, M. Copper Biocides in the Marine Environment; Arai, T., Harino, H., Ohji, M., Langston, W. J., Eds.; Springer: 2009; pp. 413-431.
- (7) Martins, S. E.; Fillmann, G.; Lillicrap, A.; Thomas, K. V. Review: Ecotoxicity of Organic and Organo-Metallic Antifouling Co-Biocides and Implications for Environmental Hazard and Risk Assessments in Aquatic Ecosystems. Biofouling 2018, 34, 34-52.
- (8) Thomas, K. The Environmental Fate and Behaviour of Antifouling Paint Booster Biocides: A Review. Biofouling 2001, 17, 73 - 86
- (9) Oliveira, I. B.; Groh, K. J.; Schönenberger, R.; Barroso, C.; Thomas, K. V.; Suter, M. J. F. Toxicity of Emerging Antifouling Biocides to Non-Target Freshwater Organisms from Three Trophic Levels. Aquat. Toxicol. 2017, 191, 164-174.

- (10) Bellas, J. Comparative Toxicity of Alternative Antifouling Biocides on Embryos and Larvae of Marine Invertebrates. *Sci. Total Environ.* **2006**, *367*, *573*–585.
- (11) Chen, S.; Li, L.; Zhao, C.; Zheng, J. Surface Hydration: Principles and Applications toward Low-Fouling/Nonfouling Biomaterials. *Polymer* **2010**, *51*, 5283–5293.
- (12) Nurioglu, A. G.; Esteves, A. C. C.; De With, G. Non-Toxic, Non-Biocide-Release Antifouling Coatings Based on Molecular Structure Design for Marine Applications. *J. Mater. Chem. B* **2015**, 3, 6547–6570.
- (13) Holland, R.; Dugdale, T. M.; Wetherbee, R.; Brennan, A. B.; Finlay, J. A.; Callow, J. A.; Callow, M. E. Adhesion and Motility of Fouling Diatoms on a Silicone Elastomer. *Biofouling* **2004**, *20*, 323–329.
- (14) Hu, P.; Xie, Q.; Ma, C.; Zhang, G. Silicone-Based Fouling-Release Coatings for Marine Antifouling. *Langmuir* **2020**, *36*, 2170–2183
- (15) Lejars, M.; Margaillan, A.; Bressy, C. Fouling Release Coatings: A Nontoxic Alternative to Biocidal Antifouling Coatings. *Chem. Rev.* **2012**, *112*, 4347–4390.
- (16) Webster, D. C.; Bodkhe, R. B. Functionalized Silicones with Polyalkylene Oxide Side Chains. WO 2013/052181 A2, 2013.
- (17) Galhenage, T. P.; Webster, D. C.; Moreira, A. M. S.; Burgett, R. J.; Stafslien, S. J.; Vanderwal, L.; Finlay, J. A.; Franco, S. C.; Clare, A. S. Poly(Ethylene) Glycol-Modified, Amphiphilic, Siloxane—Polyurethane Coatings and Their Performance as Fouling-Release Surfaces. J. Coatings Technol. Res. 2017, 14, 307—322.
- (18) Hawkins, M. L.; Faÿ, F.; Réhel, K.; Linossier, I.; Grunlan, M. A. Bacteria and Diatom Resistance of Silicones Modified with PEO-Silane Amphiphiles. *Biofouling* **2014**, *30*, 247–258.
- (19) Martinelli, E.; Suffredini, M.; Galli, G.; Glisenti, A.; Pettitt, M. E.; Callow, M. E.; Callow, J. A.; Williams, D.; Lyall, G. Amphiphilic Block Copolymer/Poly(Dimethylsiloxane) (PDMS) Blends and Nanocomposites for Improved Fouling-Release. *Biofouling* **2011**, 27, 529–541.
- (20) Wenning, B. M.; Martinelli, E.; Mieszkin, S.; Finlay, J. A.; Fischer, D.; Callow, J. A.; Callow, M. E.; Leonardi, A. K.; Ober, C. K.; Galli, G. Model Amphiphilic Block Copolymers with Tailored Molecular Weight and Composition in PDMS-Based Films to Limit Soft Biofouling. ACS Appl. Mater. Interfaces 2017, 9, 16505–16516.
- (21) Oliva, M.; Martinelli, E.; Galli, G.; Pretti, C. PDMS-Based Films Containing Surface-Active Amphiphilic Block Copolymers to Combat Fouling from Barnacles B. amphitrite and B. improvisus. Polymer 2017, 108, 476–482.
- (22) Bodkhe, R. B.; Stafslien, S. J.; Daniels, J.; Cilz, N.; Muelhberg, A. J.; Thompson, S. E. M.; Callow, M. E.; Callow, J. A.; Webster, D. C. Zwitterionic Siloxane-Polyurethane Fouling-Release Coatings. *Prog. Org. Coat.* **2015**, *78*, 369–380.
- (23) Sun, C.; Fantner, G. E.; Adams, J.; Hansma, P. K.; Waite, J. H. The Role of Calcium and Magnesium in the Concrete Tubes of the Sandcastle Worm. *J. Exp. Biol.* **2007**, *210*, 1481–1488.
- (24) Zhao, H.; Sun, C.; Stewart, R. J.; Waite, J. H. Cement Proteins of the Tube-Building Polychaete *Phragmatopoma californica*. *J. Biol. Chem.* **2005**, 280, 42938–42944.
- (25) Waite, J. H. Mussel Adhesion Essential Footwork. *J. Exp. Biol.* **2017**, 220, 517–530.
- (26) Miller, D. R.; Spahn, J. E.; Waite, J. H. The Staying Power of Adhesion-Associated Antioxidant Activity in *Mytilus californianus*. *J. R. Soc., Interface* **2015**, *12*, 20150614.
- (27) Schultzhaus, J. N.; Wang, C.; Patel, S.; Smerchansky, M.; Phillips, D.; Taitt, C. R.; Leary, D. H.; Hervey, J.; Dickinson, G. H.; So, C. R.; Scancella, J. M.; Wahl, K. J.; Spillmann, C. M. Distribution of Select Cement Proteins in the Acorn Barnacle *Amphibalanus amphitrite. Front. Mar. Sci.* **2020**, DOI: 10.3389/fmars.2020.586281.
- (28) Aldred, N.; Chan, V. B. S.; Emami, K.; Okano, K.; Clare, A. S.; Mount, A. S. Chitin Is a Functional Component of the Larval Adhesive of Barnacles. *Commun. Biol.* **2020**, *3*, 1–8.
- (29) So, C. R.; Scancella, J. M.; Fears, K. P.; Essock-Burns, T.; Haynes, S. E.; Leary, D. H.; Diana, Z.; Wang, C.; North, S.; Oh, C. S.;

- Wang, Z.; Orihuela, B.; Rittschof, D.; Spillmann, C. M.; Wahl, K. J. Oxidase Activity of the Barnacle Adhesive Interface Involves Peroxide-Dependent Catechol Oxidase and Lysyl Oxidase Enzymes. *ACS Appl. Mater. Interfaces* **2017**, *9*, 11493–11505.
- (30) Fears, K. P.; Orihuela, B.; Rittschof, D.; Wahl, K. J. Acorn Barnacles Secrete Phase-Separating Fluid to Clear Surfaces Ahead of Cement Deposition. *Adv. Sci.* **2018**, *5*, 1700762.
- (31) Kamino, K.; Inoue, K.; Maruyama, T.; Takamatsu, N.; Harayama, S.; Shizuri, Y. Barnacle Cement Proteins: Importance of Disulfide Bonds in Their Insolubility. *J. Biol. Chem.* **2000**, 275, 27360–27365.
- (32) Lachnit, M.; Buhmann, M. T.; Klemm, J.; Kröger, N.; Poulsen, N. Identification of Proteins in the Adhesive Trails of the Diatom *Amphora coffeaeformis. Philos. Trans. R. Soc., B* **2019**, 374, 20190196.
- (33) Del Grosso, C. A.; McCarthy, T. W.; Clark, C. L.; Cloud, J. L.; Wilker, J. J. Managing Redox Chemistry to Deter Marine Biological Adhesion. *Chem. Mater.* **2016**, 28, 6791–6796.
- (34) Nicolas, J.; Guillaneuf, Y.; Lefay, C.; Bertin, D.; Gigmes, D.; Charleux, B. Nitroxide-Mediated Polymerization. *Prog. Polym. Sci.* **2013**, *38*, 63–235.
- (35) Tebben, L.; Studer, A. Nitroxides: Applications in Synthesis and in Polymer Chemistry. *Angew. Chem., Int. Ed.* **2011**, *50*, 5034–5068.
- (36) Soule, B. P.; Hyodo, F.; Matsumoto, K.-I.; Simone, N. L.; Cook, J. A.; Krishna, M. C.; Mitchell, J. B. The Chemistry and Biology of Nitroxide Compounds. *Free Radical Biol. Med.* **2007**, *42*, 1632–1650.
- (37) Prescott, C.; Bottle, S. E. Biological Relevance of Free Radicals and Nitroxides. *Cell Biochem. Biophys.* **2017**, 75, 227–240.
- (38) Tomlinson, E. P.; Hay, M. E.; Boudouris, B. W. Radical Polymers and Their Application to Organic Electronic Devices. *Macromolecules* **2014**, 47, 6145–6158.
- (39) de la Fuente-Núñez, C.; Reffuveille, F.; Fairfull-Smith, K. E.; Hancock, R. E. W. Effect of Nitroxides on Swarming Motility and Biofilm Formation, Multicellular Behaviors in *Pseudomonas aeruginosa*. *Antimicrob. Agents Chemother.* **2013**, *57*, 4877–4881.
- (40) Alexander, S. A.; Rouse, E. M.; White, J. M.; Tse, N.; Kyi, C.; Schiesser, C. H. Controlling Biofilms on Cultural Materials: The Role of 3-(Dodecane-1-Thiyl)-4-(Hydroxymethyl)-2,2,5,5-Tetramethyl-1-Pyrrolinoxyl. Chem. Commun. 2015, 51, 3355–3358.
- (41) Alexander, S. A.; Kyi, C.; Schiesser, C. H. Nitroxides as Anti-Biofilm Compounds for the Treatment of *Pseudomonas aeruginosa* and Mixed-Culture Biofilms. *Org. Biomol. Chem.* **2015**, *13*, 4751–4759.
- (42) Boase, N. R. B.; Torres, M. D. T.; Fletcher, N. L.; de la Fuente-Nunez, C.; Fairfull-Smith, K. E. Polynitroxide Copolymers to Reduce Biofilm Fouling on Surfaces. *Polym. Chem.* **2018**, *9*, 5308–5318.
- (43) Heckler, I.; Boon, E. M. Insights Into Nitric Oxide Modulated Quorum Sensing Pathways. *Front. Microbiol.* **2019**, DOI: 10.3389/fmicb.2019.02174.
- (44) Saito, K.; Takeshita, K.; Ueda, J. I.; Ozawa, T. Two Reaction Sites of a Spin Label, TEMPOL (4-Hydroxy-2,2,6,6-Tetramethylpiperidine-N-Oxyl), with Hydroxyl Radical. *J. Pharm. Sci.* **2003**, *92*, 275–280.
- (45) Samuni, A.; Goldstein, S.; Russo, A.; Mitchell, J. B.; Krishna, M. C.; Neta, P. Kinetics and Mechanism of Hydroxyl Radical and OH-Adduct Radical Reactions with Nitroxides and with Their Hydroxylamines. *J. Am. Chem. Soc.* **2002**, *124*, 8719–8724.
- (46) Asmus, K. D.; Nigam, S.; Willson, R. L. Kinetics of Nitroxyl Radical Reactions a Pulse-Radiolysis Conductivity Study. *Int. J. Radiat. Biol.* **1976**, 29, 211–219.
- (47) Goldstein, S.; Samuni, A. Kinetics and Mechanism of Peroxyl Radical Reactions with Nitroxides. *J. Phys. Chem. A* **2007**, *111*, 1066–1072.
- (48) Bowry, V. W.; Ingold, K. U. Kinetics of Nitroxide Radical Trapping. 2. Structural Effects. *J. Am. Chem. Soc.* **1992**, *114*, 4992–4996.
- (49) Chateauneuf, J.; Lusztyk, J.; Ingold, K. U. Absolute Rate Constants for the Reactions of Some Carbon-Centered Radicals with 2,2,6,6-Tetramethyl-1-piperidinoxyl. *J. Org. Chem* **1988**, 53, 1629–1632.

- (50) Beckwith, A. L. J.; Bowry, V. W.; O'Leary, M.; Moad, G.; Rizzardo, E.; Solomon, D. H. Kinetic Data for Coupling of Primary Alkyl Radicals with a Stable Nitroxide. *J. Chem. Soc., Chem. Commun.* 1986, 1003–1004.
- (51) Goldstein, S.; Samuni, A.; Merenyi, G. Kinetics of the Reaction between Nitroxide and Thiyl Radicals: Nitroxides as Antioxidants in the Presence of Thiols. *J. Phys. Chem. A* **2008**, *112*, 8600–8605.
- (52) Calabrese, D. R.; Wenning, B.; Finlay, J. A.; Callow, M. E.; Callow, J. A.; Fischer, D.; Ober, C. K. Amphiphilic Oligopeptides Grafted to PDMS-Based Diblock Copolymers for Use in Antifouling and Fouling Release Coatings. *Polym. Adv. Technol.* **2015**, *26*, 829–836.
- (53) Calabrese, D. R.; Wenning, B. M.; Buss, H.; Finlay, J. A.; Fischer, D.; Clare, A. S.; Segalman, R. A.; Ober, C. K. Oligopeptide-Modified Hydrophobic and Hydrophilic Polymers as Antifouling Coatings. *Green Mater.* **2017**, *5*, 31–43.
- (54) Patterson, A. L.; Wenning, B.; Rizis, G.; Calabrese, D. R.; Finlay, J. A.; Franco, S. C.; Zuckermann, R. N.; Clare, A. S.; Kramer, E. J.; Ober, C. K.; Segalman, R. A. Role of Backbone Chemistry and Monomer Sequence in Amphiphilic Oligopeptide- and Oligopeptoid-Functionalized PDMS- and PEO-Based Block Copolymers for Marine Antifouling and Fouling Release Coatings. *Macromolecules* **2017**, *50*, 2656–2667.
- (55) Barry, M. E.; Davidson, E. C.; Zhang, C.; Patterson, A. L.; Yu, B.; Leonardi, A. K.; Duzen, N.; Malaviya, K.; Clarke, J. L.; Finlay, J. A.; Clare, A. S.; Chen, Z.; Ober, C. K.; Segalman, R. A. The Role of Hydrogen Bonding in Peptoid-Based Marine Antifouling Coatings. *Macromolecules* **2019**, *52*, 1287–1295.
- (56) Wenzel, R. N. Resistance of Solid Surfaces to Wetting by Water. *Ind. Eng. Chem.* **1936**, 28, 988–994.
- (57) Weinman, C. J.; Finlay, J. A.; Park, D.; Paik, M. Y.; Krishnan, S.; Sundaram, H. S.; Dimitriou, M.; Sohn, K. E.; Callow, M. E.; Callow, J. A.; Handlin, D. L.; Willis, C. L.; Kramer, E. J.; Ober, C. K. ABC Triblock Surface Active Block Copolymer with Grafted Ethoxylated Fluoroalkyl Amphiphilic Side Chains for Marine Antifouling/Fouling-Release Applications. *Langmuir* 2009, 25, 12266–12274.
- (58) Aldred, N.; Li, G.; Gao, Y.; Clare, A. S.; Jiang, S. Modulation of Barnacle (*Balanus amphitrite* Darwin) Cyprid Settlement Behavior by Sulfobetaine and Carboxybetaine Methacrylate Polymer Coatings. *Biofouling* **2010**, *26*, 673–683.
- (59) Guillard, R. R.; Ryther, J. H. Studies of Marine Planktonic Diatoms. I. *Cyclotella nana* Hustedt, and *Detonula confervacea* (Cleve) Gran. *Can. J. Microbiol.* **1962**, *8*, 229–239.
- (60) Schultz, M. P.; Finlay, J. A.; Callow, M. E.; Callow, J. A. A Turbulent Channel Flow Apparatus for the Determination of the Adhesion Strength of Microfouling Organisms. *Biofouling* **2000**, *15*, 243–251.
- (61) Callow, M. E.; Callow, J. A.; Pickett-Heaps, J. D.; Wetherbee, R. Primary Adhesion of *Enteromorpha* (Chlorophyta, Ulvales) Propagules: Quantitative Settlement Studies and Video Microscopy. *J. Phycol.* **1997**, 33, 938–947.
- (62) Starr, R. C.; Zeikus, J. A. UTEX-The Culture Collection of Algae at the University of Texas at Austin 1993 List of Cultures. *J. Phycol.* **1993**, 29, 1–106.
- (63) Turkmen, S.; Atlar, M.; Yeginbayeva, I.; Benson, S.; Finlay, J. A.; Clare, A. S. Frictional Drag Measurements of Large-Scale Plates in an Enhanced Plane Channel Flowcell. *Biofouling* **2020**, *36*, 169–182.
- (64) Tukey, J. W. Comparing Individual Means in the Analysis of Variance. *Biometrics* **1949**, *5*, 99–114.
- (65) Wenning, B. M. Synthesis and Study of Functionalized Poly(Dimethyl Siloxane) Block Copolymers: Control of Surface Properties and Use in Antibiofouling Coatings; Ph.D. Thesis, Cornell University: 2016
- (66) Zhang, Y.; Park, A.; Cintora, A.; McMillan, S. R.; Harmon, N. J.; Moehle, A.; Flatté, M. E.; Fuchs, G. D.; Ober, C. K. Impact of the Synthesis Method on the Solid-State Charge Transport of Radical Polymers. *J. Mater. Chem. C* **2018**, *6*, 111–118.
- (67) Bales, B. L.; Meyer, M.; Smith, S.; Peric, M. EPR Line Shifts and Line Shape Changes Due to Spin Exchange of Nitroxide Free

- Radicals in Liquids: 6. Separating Line Broadening Due to Spin Exchange and Dipolar Interactions. *J. Phys. Chem. B* **2009**, *113*, 4930–4940.
- (68) Mas-Torrent, M.; Crivillers, N.; Rovira, C.; Veciana, J. Attaching Persistent Organic Free Radicals to Surfaces: How and Why. *Chem. Rev.* **2012**, *112*, 2506–2527.
- (69) Krishnan, S.; Wang, N.; Ober, C. K.; Finlay, J. A.; Callow, M. E.; Callow, J. A.; Hexemer, A.; Sohn, K. E.; Kramer, E. J.; Fischer, D. A. Comparison of the Fouling Release Properties of Hydrophobic Fluorinated and Hydrophilic PEGylated Block Copolymer Surfaces: Attachment Strength of the Diatom *Navicula* and the Green Alga *Ulva*. *Biomacromolecules* **2006**, *7*, 1449–1462.
- (70) Youngblood, J. P.; Andruzzi, L.; Ober, C. K.; Hexemer, A.; Kramer, E. J.; Callow, J. A.; Finlay, J. A.; Callow, M. E. Coatings Based on Side-Chain Ether-Linked Poly(Ethylene Glycol) and Fluorocarbon Polymers for the Control of Marine Biofouling. *Biofouling* **2003**, *19*, 21–28
- (71) Chaudhury, M. K.; Finlay, J. A.; Chung, J. Y.; Callow, M. E.; Callow, J. A. The Influence of Elastic Modulus and Thickness on the Release of the Soft-Fouling Green Alga *Ulva linza* (Syn. *Enteromorpha linza*) from Poly(Dimethylsiloxane) (PDMS) Model Networks. *Biofouling* **2005**, 21, 41–48.
- (72) Brady, R. F., Jr.; Singer, I. L. Mechanical Factors Favoring Release from Fouling Release Coatings. *Biofouling* **2000**, *15*, 73–81.
- (73) Baek, Y.; Kang, J.; Theato, P.; Yoon, J. Measuring Hydrophilicity of RO Membranes by Contact Angles via Sessile Drop and Captive Bubble Method: A Comparative Study. *Desalination* **2012**, 303. 23–28.
- (74) Cintora, A.; Takano, H.; Khurana, M.; Chandra, A.; Hayakawa, T.; Ober, C. K. Block Copolymers Containing Stable Radical and Fluorinated Blocks with Long-Range Ordered Morphologies Prepared by Anionic Polymerization. *Polym. Chem.* **2019**, *10*, 5094–5102.
- (75) Cunha, A. V.; Salamatova, E.; Bloem, R.; Roeters, S. J.; Woutersen, S.; Pshenichnikov, M. S.; Jansen, T. L. C. Interplay between Hydrogen Bonding and Vibrational Coupling in Liquid N-Methylacetamide. *J. Phys. Chem. Lett.* **2017**, *8*, 2438–2444.
- (76) McQuade, D. T.; McKay, S. L.; Powell, D. R.; Gellman, S. H. Indifference to Hydrogen Bonding in a Family of Secondary Amides. *J. Am. Chem. Soc.* **1997**, *119*, 8528–8532.
- (77) Zhang, G.; Wong, Y.-H.; Zhang, Y.; He, L.-S.; Xu, Y.; Qian, P.-Y. Nitric Oxide Inhibits Larval Settlement in *Amphibalanus amphitrite* Cyprids by Repressing Muscle Locomotion and Molting. *Proteomics* **2015**, *15*, 3854–3864.
- (78) Dobretsov, S.; Thomason, J. C. The Development of Marine Biofilms on Two Commercial Non-Biocidal Coatings: A Comparison between Silicone and Fluoropolymer Technologies. *Biofouling* **2011**, 27, 869–880.
- (79) Yandi, W.; Mieszkin, S.; di Fino, A.; Martin-Tanchereau, P.; Callow, M. E.; Callow, J. A.; Tyson, L.; Clare, A. S.; Ederth, T. Charged Hydrophilic Polymer Brushes and Their Relevance for Understanding Marine Biofouling. *Biofouling* **2016**, *32*, 609–625.
- (80) Heydt, M.; Pettitt, M. E.; Cao, X.; Callow, M. E.; Callow, J. A.; Grunze, M.; Rosenhahn, A. Settlement Behavior of Zoospores of *Ulva linza* during Surface Selection Studied by Digital Holographic Microscopy. *Biointerphases* **2012**, *7*, 33.
- (81) Finlay, J. A.; Schultz, M. P.; Cone, G.; Callow, M. E.; Callow, J. A. A Novel Biofilm Channel for Evaluating the Adhesion of Diatoms to Non-Biocidal Coatings. *Biofouling* **2013**, *29*, 401–411.
- (82) Thompson, S. E. M.; Taylor, A. R.; Brownlee, C.; Callow, M. E.; Callow, J. A. The Role of Nitric Oxide in Diatom Adhesion in Relation to Substratum Properties. *J. Phycol.* **2008**, *44*, 967–976.
- (83) Dolch, L. J.; Lupette, J.; Tourcier, G.; Bedhomme, M.; Collin, S.; Magneschi, L.; Conte, M.; Seddiki, K.; Richard, C.; Corre, E.; Fourage, L.; Laeuffer, F.; Richards, R.; Reith, M.; Rébeillé, F.; Jouhet, J.; McGinn, P.; Maréchal, E. Nitric Oxide Mediates Nitrite-Sensing and Acclimation and Triggers a Remodeling of Lipids. *Plant Physiol.* 2017, 175, 1407–1423.